IEEE Access
Multidisciplinary ⋮ Rapid Review ⋮ Open Access Journal

Received 26 February 2024, accepted 25 March 2024, date of publication 1 April 2024, date of current version 30 April 2024.

Digital Object Identifier 10.1109/ACCESS.2024.3383545

APPLIED RESEARCH

Novel Pulsed WPT System With Data Transfer Capability for Condition Monitoring of Industrial Rotating Equipment

RAFFAELE SALVATI, (Member, IEEE), VALENTINA PALAZZI, (Senior Member, IEEE), FEDERICO ALIMENTI, (Senior Member, IEEE), PAOLO MEZZANOTTE, (Member, IEEE), ANTONIO FABA, (Senior Member, IEEE), ERMANNO CARDELLI, (Senior Member, IEEE), AND LUCA ROSELLI, (Fellow, IEEE)

Department of Engineering, University of Perugia, 06125 Perugia, Italy

Corresponding author: Raffaele Salvati (raffaele.salvati@studenti.unipg.it)

This work was supported in part by Electronic Component Systems for European Leadership (ECSEL) Joint Undertaking (JU) under Grant 876362; in part by JU receives support from European Union's Horizon 2020 Research and Innovation Program and Finland, Austria, Belgium, Czechia, Germany, Italy, Latvia, The Netherlands, Poland, and Switzerland; and in part by the University of Perugia in the frame of the Basic Research Program, in 2017 and 2018.

ABSTRACT In this paper, we present a 6.78 MHz Pulsed Wireless Power Transfer (PWPT) system specifically designed for powering the electronics placed on a suction roll of a paper mill machinery, thus enabling rotating equipment monitoring. The system utilizes a pair of different resonant coils to maintain a stable coupling coefficient for a fraction of the roll rotation period while guaranteeing compactness and ease of installation. Designed using both Commercial-off-the-Shelf (COTS) and custom components, the developed WPT system achieves a DC-DC efficiency of 62% in the specific working conditions. The transferred power is used to supply an Internet-of-Things (IoT) node that continuously measures and transmits data about the operation status. A fully operational system for battery and angular position monitoring has been developed and tested in a laboratory environment. This research presents a comprehensive analysis of the system and explores the interaction of different coils to maintain a stable coupling coefficient in dynamic applications. The same approach can be employed for rotating machinery with similar geometrical constraints or more general dynamic applications characterized by periodic movements and limited space for the coupling system.

INDEX TERMS WPT, coils, Bluetooth low-energy, condition monitoring, DC-DC efficiency, IIoT, supercapacitors.

I. INTRODUCTION

Recently, the field of Wireless Power Transfer (WPT) has seen remarkable advancements, leading to its application across various sectors, including medical devices, electric vehicles, consumer electronics, and more [1], [2], [3], [4], [5], [6], [7]. The appeal of WPT lies in its ability to provide alternative power supply solutions, particularly to devices with spatial constraints such as wearable gadgets, mobile devices, distributed monitoring networks and so forth; where traditional power supply options like cables or batteries may be cumbersome or impractical [8], [9], [10], [11]. In industrial settings, the synergy between WPT systems and Wireless Sensor Networks (WSNs) enhances the robustness of condition monitoring systems [12], [13]. In application with moving or rotating parts, batteries and cables are subject to material degradation and mechanical fatigue over time, leading to frequent replacements and machinery shutdowns, thus resulting in high maintenance costs and manufacturing rate reduction [14], [15]. By integrating WPT and WSNs,

The associate editor coordinating the review of this manuscript and approving it for publication was Gongbo Zhou.

the system facilitates predictive maintenance through real-time data analytics. This not only streamlines maintenance schedules but also minimizes downtime and operational costs [16], [17], [18].

WPT systems for dynamic applications have been extensively treated in the scientific literature. Typically, WPT systems utilize multiple coils in transmission or reception to increase the effective charging area while geometry optimization techniques are implemented to reduce the efficiency drop caused by misalignment [19], [20], [21], [22], [23], [24], [25], [26], [27], [28]. In [21] coil arrays are employed on the transmitting side to form a large 100 kHz charging area for electric wheelchairs. Although free-positioning and high efficiency are achieved, the transmitter area is 0.75 m^2 and uses three coil layers stacked one above the other. Moreover, controllers are needed to detect the device and optimize WPT operation. A spatially-shifted overlapped Double-D (DD) coil array system is proposed in [22] for powering a moving target. Overlapped DD coils can generate a stable magnetic flux between the transmitter and the receiver, but they require additional components and a controller, thereby increasing system cost and complexity. Reference [25] introduces an omnidirectional WPT system that employs a 3D coil to achieve angular misalignment insensitivity. However, this 3D structure might not be suitable for many applications, especially those with strict geometrical constraints where planar coils are preferred or even mandatory. Industrial machinery, in fact, are often composed of multiple blocks that may not always accommodate large coupling systems, thus requiring customized design solutions for compact and effective WPT implementations.

In this paper, we propose a novel Pulsed Wireless Power Transfer (PWPT) system specifically designed to enable condition monitoring on paper mill machinery. A pair of coils with different geometries are placed on the static and rotating part of a metallic roll, enabling power transfer through magnetic coupling for a fraction of the rotation period during each revolution. By employing coils with different geometries the coupling coefficient is maintained constant for a wide rotation angle. The proposed system operates inside the 6.78 MHz ISM band [29]. This frequency improves the coupling performance of the coil system and allows for a reduction in the size of the coils [30]. The energy transferred through WPT is utilized to power an Internet of Things (IoT) node placed on the roll, equipped with a Microcontroller Unit (MCU) and a Bluetooth Low-Energy (BLE) transceiver. The node is responsible for monitoring and transmitting data about the energy storage device status and its real-time angular position, and thus of the roll. Transmitted data are received by another MCU placed on the static side, which forwards them to a computer for processing operations.

The fully operational system is presented, analysed, and tested in a laboratory environment using rotating emulating equipment. This research offers an extensive study of a WPT system using coils with different geometries. The findings are applicable to industrial environments with similar conditions, as well as to more general applications constrained by similar geometry and dynamics.

II. SYSTEM OVERVIEW

Fig. 1 illustrates the block diagram of the developed monitoring system. The WPT system consists of two inductively coupled resonators, a Commercial-Off-The-Shelf (COTS) Power Amplifier (PA), and an AC/DC stage. The WPT system supplies an IoT node consisting of an MCU equipped with a BLE transceiver and various sensors. In this configuration, the WPT transmitter and one MCU with a BLE transceiver are static, while the WPT receiver and the node are placed on a rotating roll. The primary objective of the WPT system is to supply sufficient energy to the IoT node, enabling continuous condition monitoring while ensuring compactness and ease of installation. For this purpose, a coil system consisting of two coupled resonant coils has been designed, where the two coils overlap for a fraction of the rotation period of the roll.

First, the IoT node is described and the energy requirements analysis of the system is presented. Subsequently, each block is described and characterized in detail (Sec. III). Finally, the performance of the entire system, operating under dynamic conditions, is reported (Sec. IV).

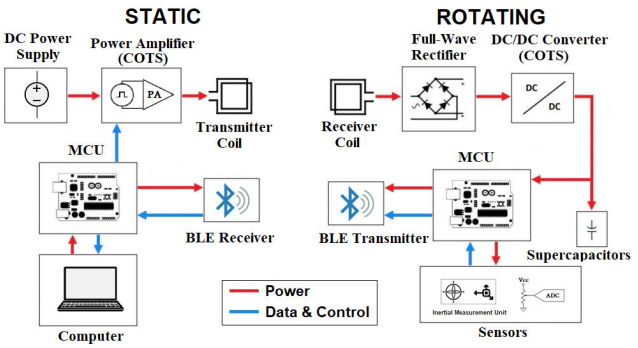

FIGURE 1. Block diagram of the designed wireless power transfer system with data transfer capability for rotating applications.

A. MCU NODE

The chosen MCU board for this application is an Arduino Nano 33 BLE. It is equipped with an Inertial Measurement Unit (IMU) to perform angle measurement, a BLE module to wirelessly transmit data, and several Analog-to-Digital Converters (ADCs) accessible via analog inputs. The node can operate with external supply voltages in the range of 4-21 V but in this application, the maximum voltage value is set to 5 V. This value was chosen since it is a common voltage level used in many electronic systems, including microcontrollers, sensors, and other peripherals. Moreover, it can be easily adjusted to 3.3 V using a voltage regulator. The node is also provided with LEDs as visual feedback on the status of the operation. The node schematic is shown

in Fig. 2 (a). The supply voltage is constantly monitored using one of the available analog input pins. Since the MCU circuitry operates at 3.3 V, a resistive voltage divider is used to scale the ADC input voltage by a factor $\alpha_v = 0.658$, resistance values (i.e. R1 and R2) are reported in the schematic. The MCU angular orientation is measured by leveraging the 3D gyroscope and accelerometer sensors in the onboard IMU. Digital data received from these sensors are combined inside the MCU using a digital complementary filter to evaluate roll angular position. This simple but effective sensor fusion technique helps to reduce the major drawbacks of the employed sensors. Gyroscopes, in fact, tend to drift over time due to noise or bias, and accelerometers are affected as well by noise and linear acceleration [31].

A custom BLE service with two BLE characteristics is used to transmit data. Each characteristic, one for the supply voltage and the other for angular position data has a payload of 2 bytes and uses the notify mechanism. Indeed, whenever new data is ready to be sent, the node notifies the other MCU, which, in turn, initiates the reading procedure. Fig. 2 (b) shows the flux diagram describing the operation of the IoT node, which operates continuously as long as its supply voltage is above 4 V. The power consumption of the IoT node was estimated by measuring the drained current with different supply voltages when fully operational, i.e. reading and transmitting data, using a digital multimeter (model 34401A from Agilent, accuracy 0.01 %). The power consumption slightly increases with V_{load} due to the internal regulator connected to the Vin pin. Specifically, as the Arduino operates at 3.3 V, at higher V_{load} there is an increase in the power dissipated due to the larger voltage step-down. The measured I-V pairs are reported in Table 1.

TABLE 1. Estimated power consumption of the IoT node by measuring the drained current for various supply voltage values.

IoT Node Power Consumption			
V_{load} (V)	I_{node} (mA)	P_{node} (mW)	R_{node} (Ω)
4.0	74.29	297.2	54
4.3	70.2	301.9	61
4.6	68.4	314.6	67
5.0	65.00	325.0	77

B. ENERGY CONSIDERATION

By definition, the system DC-DC efficiency is:

$$\eta_{wpt} = \frac{P_{load}}{P_{in}} = \eta_{amp} \cdot \eta_{coil} \cdot \eta_{rect} \cdot \eta_{buck} \tag{1}$$

where P_{in} is the PA DC input power, η_{amp} is the PA DC-RF efficiency, η_{coil} is the coil system transmission efficiency, η_{rect} is the rectifier RF-DC efficiency, and η_{buck} is the buck converter efficiency. Assuming T_{rev} be the revolution period of the roll, the node consumes an amount of energy equal to $E_{rev} = P_{node} \times T_{rev}$ J during each revolution. The WPT system must be able to deliver to the load the energy E_{rev} only while the coils are overlapped, thus resulting in an increased

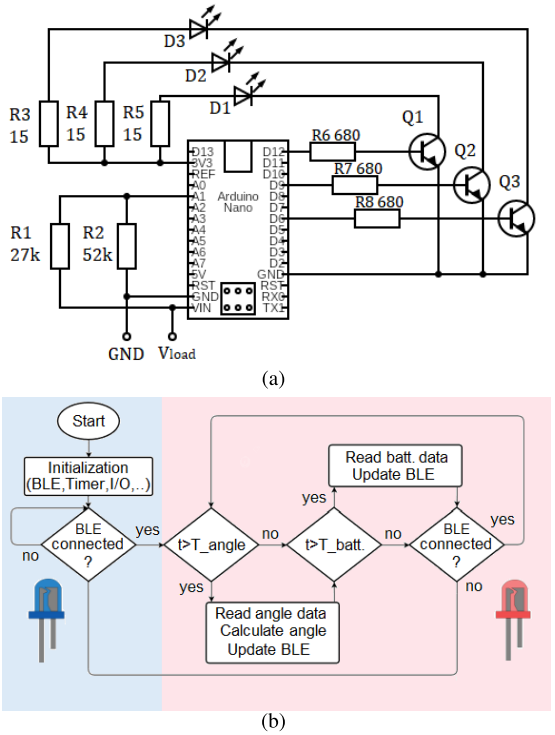

FIGURE 2. IoT node for supply voltage and angular orientation real-time monitoring. (a) Schematic, and (b) operations flowchart.

transmitted power compared to a continuous transmission operation. The energy balance is reached when

$$P_{load} \cdot T_{tx} = P_{node} \cdot T_{rev} \tag{2}$$

$$T_{tx} = \frac{T_{rev}}{\chi}; \quad \chi = \frac{360}{\alpha} \tag{3}$$

thus

$$P_{in} \cdot T_{tx} \cdot \eta_{wpt} = P_{node} \cdot T_{rev} \tag{4}$$

where T_{tx} is the wireless power transmission interval corresponding to an angular range α during each revolution and assuming the system transmission efficiency η_{wpt} constant during T_{tx}. Therefore, the required input power for the PA can be calculated as

$$P_{in} = \frac{\chi \cdot P_{node}}{\eta_{wpt}} \tag{5}$$

with $\chi \cdot P_{node} = P_{load}$. Therefore, the WPT system has to deliver a power P_{load} at least χ times greater than P_{node} to supply the node for T_{tx} and store inside the supercapacitors an amount of energy δE_{cap} greater than $P_{node} \cdot (T_{rev} - T_{tx})$ to supply the node for the remaining revolution period, as shown in Fig. 3 (a), and thus

$$\delta E_{cap} \geq P_{node} \cdot T_{rev} \frac{\chi - 1}{\chi}. \tag{6}$$

For the purpose of system-level analysis, particularly in the context of wireless power transfer, it may be beneficial to approximate the entire load as a load resistance R_l. This

approximation is formulated on the basis of the required power P_{load} by the overall system. Specifically,

$$P_{load}(t) = V_{load} \cdot I_{load}(t) \tag{7}$$

where I_{load} is the sum of the current to charge the capacitors I_c and the node current I_{node} during T_{tx}, as shown in Fig. 3 (b), thus the equivalent load resistance is given by

$$R_l = \frac{V_{load}^2}{\chi \cdot P_{node}}. \tag{8}$$

This R_l serves as a computational tool to represent the power consumption of the system when power is being transferred thru WPT.

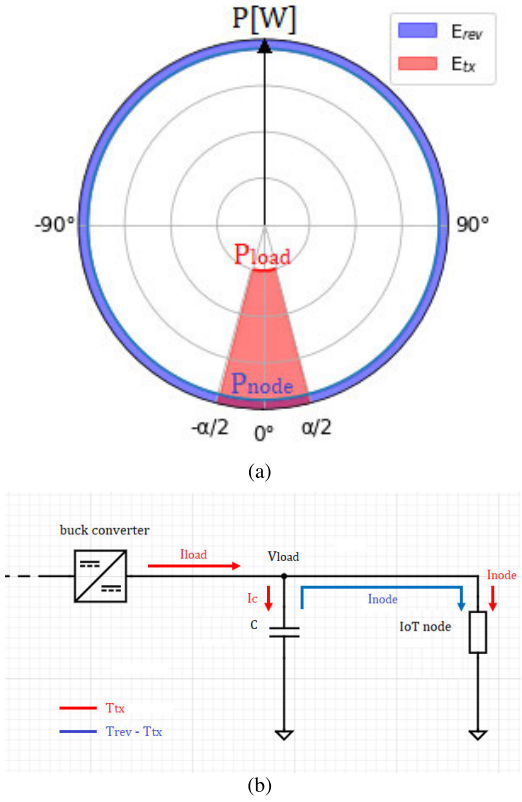

FIGURE 3. System energetic requirements. (a) Minimum power P_{load} that has to be delivered to fulfill the node energy requirement during T_{rev} (i.e. $E_{tx} = E_{rev}$). (b) Load current during an entire revolution lasting T_{rev}. During T_{tx}, the WPT system supplies the node and charges the capacitors while, for the remaining portion of the revolution, the node is supplied by the capacitors.

III. SYSTEM DESIGN AND IMPLEMENTATION

A. COUPLED INDUCTORS

The most straightforward solution to perform WPT in similar environments is to use concentric coils, one placed on the outer circle of the roll, and the other aligned with it, since this allows for constant coupling coefficient versus rotation angle. Unfortunately, this solution is not possible in our reference application, and, in general, it is not suitable for large rotating equipment due to several factors, among them, the dimension of the resulting coils and the mechanical interference of the coils with many apparatuses usually present on both rolling and stator parts (in our case, for instance, a full disc coil would interfere with the BLE transceiver). We eventually developed an alternative approach, based on compact planar coils. The coils occupy a sector of a circular crown, leaving plenty of space for the rest of the electronics. However, with this solution, we have a variable coupling coefficient, depending on the position of the rotating coil with respect to the static one. Therefore, different coils, characterized by a difference in angular coverage, have been studied to guarantee a stable coupling coefficient for a fraction of the rotation period. The dimensions of the rotating coils are limited by the dimension of the roll outer circular crown available (outer radius 30 cm, height 9 cm, and angular coverage 28° in the present case). For the static transmitting coil, similar constraints limited the available sector to 56°.

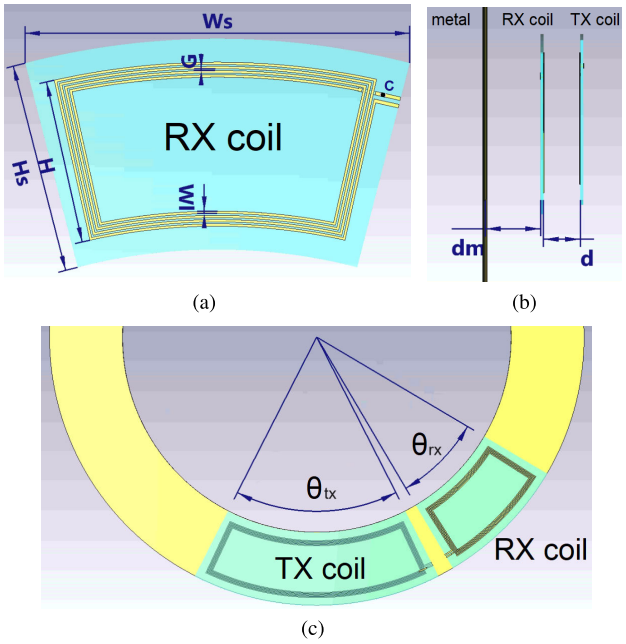

FIGURE 4. Layout of the coil system. (a) RX Coil front view, (b) coil system lateral view, and (c) coil system front view. Main parameters: Wl = 1.0 mm, G = 0.8 mm, H = 70.0 mm, Hs = 90.0 mm, d = 20.0 mm, dm= 30 mm, and t = 1.6 mm. TX coil: $\theta_{tx} = 56°$, Ws = 300 mm, C= 80 pF. RX coil: $\theta_{rx} = 28°$, Ws = 164.4 mm, C= 160 pF.

The design of the resonant coil system was conducted through electromagnetic simulations using CST Studio Suite [32]. The coils are designed on a 1.6 mm thick FR-4 substrate ($\epsilon_r = 4.7$, $tan\delta = 0.011$). As the roll is made with metal, the receiving coil lies in close proximity to a metal surface, which impacts the WPT performance. Therefore, the metal plane was included in the RX coil model. To achieve a high coupling coefficient while keeping a low parasitic series resistance, four-turn coils are chosen, as shown in Fig. 4 (a). Fig. 4 (b) illustrates the lateral view of the whole system. The separation between the coils is constant, and it is set to 2 cm mainly due to industrial constraints. The distance *dm* between

the RX coil and the metal roll behind it is set to 3 cm, which is also the maximum available space. The coupling coefficient k between the coils is calculated as follows

$$k(\theta) = \frac{M(\theta)}{\sqrt{L_1 L_2}}, \tag{9}$$

where M is the mutual coupling between the coils (which varies with the rotation angle θ), L_1 is the inductance associated with TX coil and L_2 is the inductance associated with RX coil. The mutual inductance M between two moving planar coils can be calculated based on the coil geometrical parameters using the solution of the Neumann equation [33]:

$$M(\theta) = \rho \sum_{i=1}^{n_p} \sum_{j=1}^{n_s} M_{ij}(\theta) \tag{10}$$

where M_{ij} represents the mutual coupling between the i-th spire of the primary coil and the j-th spire of the secondary, and ρ takes into account the area variation compared to circular coils.

Three coil prototypes with different angle coverage were designed and manufactured, as shown in Fig. 5 (a). Coil parameters are summarized in Table 2. The coupling coefficient between different pairs of coils was measured at various relative rotation angles and compared against electromagnetic simulations. For angular characterization, the coils were positioned within two 3D printed holders, with the receiving coil placed on a rotating moke-up. They were then connected to the two ports of a Vector Network Analyzer (VNA) (Rhode & Schwarz ZNH26). The angular position of the receiver coil was measured with the IoT node, powered by an external power supply (CPX400DP model from PowerFlex). Fig. 6 shows the comparison between the measured and simulated coupling coefficients for all combinations of coils. The RX coil was moved within an angular range of ±40°, with the position θ=0° being the perfect alignment with the TX coil. The measurements agree fairly well with the simulation results. In the case of identical spirals covering 28°, we obtain the maximum coupling coefficient (equal to 0.25); but, as expected, it occurs only when the spirals are aligned (θ=0°), while it sharply decreases as the misalignment increases. The solution θ_{tx}=56° and θ_{rx}=28° represents the best trade-off between a high coupling coefficient and a fraction of the rotation period in which the coupling coefficient is approximately constant. Indeed, k is approximately equal to 0.2 for an angle of 25°. If a smaller RX coil is chosen, the rotation period in which we can stably transfer power is a little broader (about 40° instead of 25°), but in that case, the coupling coefficient is significantly lower (0.13 instead of 0.2), as shown in Fig. 6.

A series-series compensation topology, shown in Fig. 7, was selected for the coil system to achieve resonance at 6.78 MHz. In this configuration, the resonant condition depends solely on the coil inductances and compensation capacitances. Therefore, when the coils are aligned, the resonant frequency of the coupling system is independent

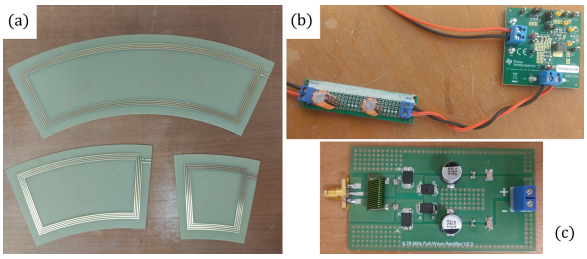

FIGURE 5. Prototypes of the WPT system. (a) Manufactured coils, (b) COTS buck converter connected in parallel to the series of two 5 F supercapacitors, and (c) IMN and full-wave rectifier.

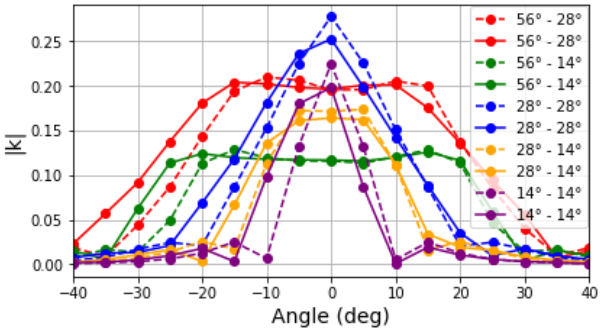

FIGURE 6. Comparison of the measured and simulated coupling coefficient for different pairs of coils (θ_{tx} - θ_{rx}) and angles. The dashed lines correspond to simulations and the solid lines to measurements.

of M and R_l [34]. The two series lumped capacitors are calculated as:

$$C_x = \frac{1}{4\pi^2 f_r^2 L_x} \tag{11}$$

where C_x and L_x are the series capacitance and coil inductance of the TX and RX coils, respectively. Table 2 reports the comparison between the simulated and measured inductance values and the respective series capacitances.

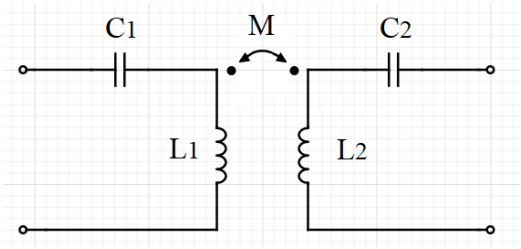

FIGURE 7. Series-series compensation topology.

The chosen configuration was also simulated for misalignment along the vertical axis that can arise during installation. Fig. 8 (a) reports the mutual inductance variation for a vertical misalignment up to 11%. Fig. 8 (b) shows the comparison of transmission coefficients for a misalignment up to 11%. The coefficient variation in the angular range ±15° is lower than 0.2 dB, which corresponds to an efficiency drop of less than 5%.

TABLE 2. Summary of the parameters for the three types of designed coils.

Coils Parameters					
θ (deg)	N	W_s (mm)	$L_{sim}(\mu H)$	$L_{meas}(\mu H)$	$C(pF)$
56	4	300.0	6.84	7.84	72
28	4	164.4	3.44	3.84	160
14	4	93.3	2.03	2.20	235

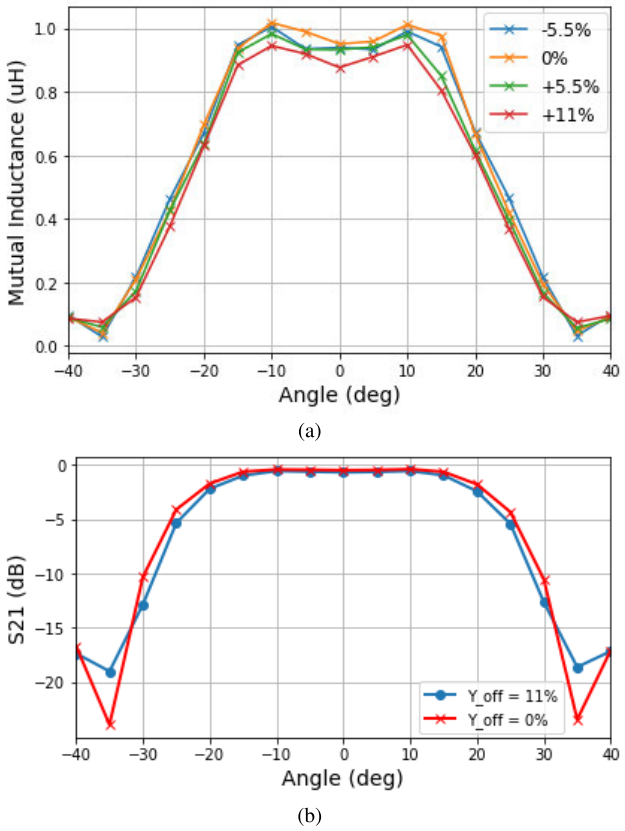

FIGURE 8. Simulations for vertical misalignment using the couple "$\theta_{tx} = 56°$ and $\theta_{rx} = 28°$. (a) mutual inductance M for various misalignment values, and (b) transmission coefficient for the best and worst cases, i.e. coil aligned and 11% of vertical misalignment.

B. DC/AC AND AC/DC CONVERSION

The chosen power amplifier for the application is the GSWP050W-EVBPA from GaN Systems, a 50 W class EF2 power amplifier based on a push-pull topology. The module includes control ports to switch the PA on and off and features a max efficiency η_{amp} of 91% according to the component datasheet. The RF signal transmitted to the rotating side is converted to a DC power supply by the AC/DC stage shown in Fig. 5. The full-wave rectifier converts the RF signal received by the RX coil to a DC voltage while the DC/DC buck converter module stabilizes the voltage to ensure a steady supply of power. The final block, the supercapacitors, acts as an energy storage device, allowing the system to store and release energy when needed.

The employed DC-DC converter is the TPS62933EVM from Texas Instruments. The module consists of a high-efficiency synchronous buck converter with a maximum output current of 3 A and input voltages ranging from 3.8 V to 30 V. To power supply the node, the output target voltage was set to 5 V by means of external resistors. A series of two 5 F supercapacitors are connected in parallel to the node, thus the buck converter output current is shared between the capacitors and the node when the coils are aligned. Conversely, when the coils are not aligned and no power is being transferred, the current flows from the capacitors to the node until the roll completes its rotation and a new pulse of power is transferred. This routine holds if the output voltage is greater than 4 V and the node is operating. During the startup, when the load voltage is lower than 4 V, all the current flows into the capacitors and no power is absorbed by the node. Therefore, the capacitors will charge up to the threshold voltage and then start supplying the node. The value of the supercapacitors was selected to ensure a stable supply voltage for the node, while also allowing for rapid charging. The adopted supercapacitors allow the system to quickly complete the startup phase, thus minimizing downtime.

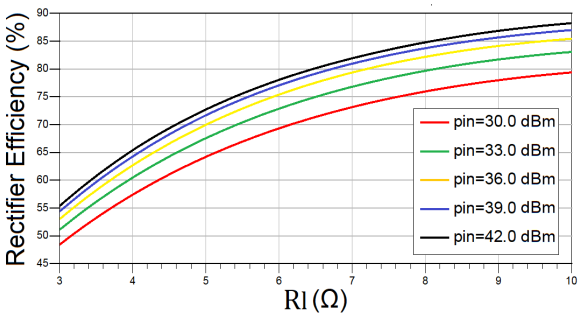

FIGURE 9. Simulated RF to DC efficiency of the full-wave rectifier for varying loads and input power levels.

The rectifier is a full-wave rectifier based on four Schottky diodes (PMEG045T030EPDZ from Nexperia), designed using Harmonic Balance simulations within Advanced Design Systems [35]. The device also includes an Input Matching Network (IMN) so that the input impedance of the rectifier can be set to maximize the power transfer efficiency of the coil system. The circuit components are $L_p = 500$ nH and $C_s = 3.55$ nF for the IMN, while the smoothing output capacitance consists of three capacitors in parallel, with size 300 uF, 0.2 uF, and 0.1 uF. The load resistance of the rectifier is calculated using (8) with a supply voltage of 5 V and the node power consumption of 325 mW, thus obtaining a value of 6.4 Ω. The simulated RF to DC efficiency is shown in Fig. 9 for a wide range of input power and different loads. It can be seen that for the target value the efficiency η_{rect} is about 75% for an input power greater than 36 dBm.

C. SYSTEM CHARACTERIZATION

To properly characterize the dynamic behavior of the WPT system, the RX coil was mounted on a roll moke-up with the same geometrical constraints of the addressed application.

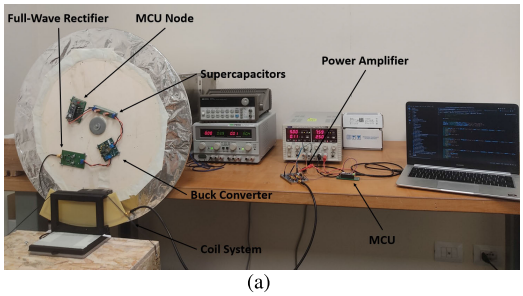

(a)

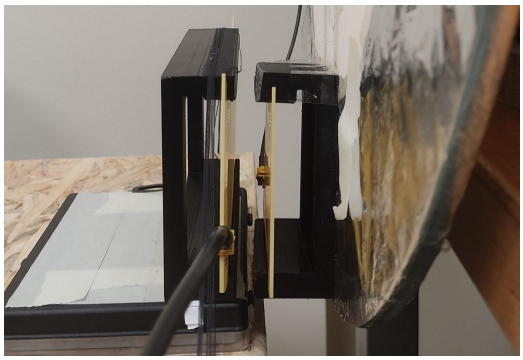

(b)

FIGURE 10. (a) Experimental setup for the wireless power and data transfer system, and (b) lateral view of the different coil system with a gap of 2 cm.

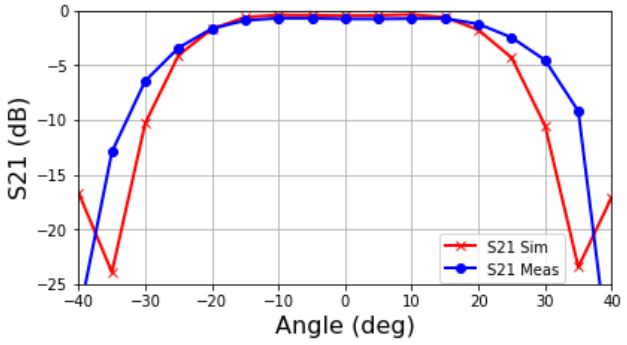

(a)

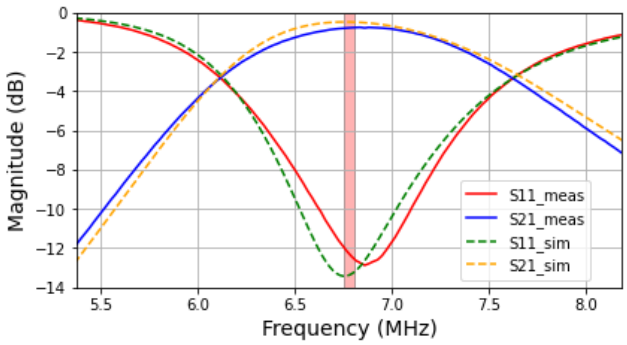

(b)

FIGURE 11. Comparison of the measured and simulated coil system S-Parameters using the couple "$\theta_{tx} = 56°$ and $\theta_{rx} = 28°$. (a) Transmission coefficient for different angles, and (b) S-parameters for $\theta = 0°$.

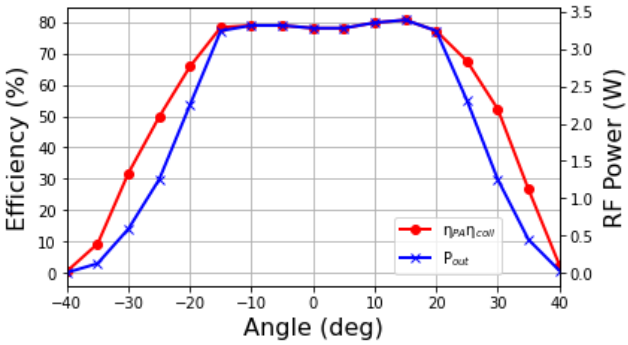

FIGURE 12. Measured efficiency and delivered power to a 50Ω load connected directly to the RX coil.

The moke-up consists of a motor connected to a wooden roll with a radius of r = 30 cm and its outer circle is covered by aluminum foils, as shown in Fig. 10 (a).

The transmission coefficient versus relative rotation angle for the coil system was measured with a VNA and compared to the simulation, as shown in Fig. 11. The measured transmission coefficient for a rotation angle of ±15° is almost flat and equal to -0.78 dB, thus achieving a power transfer efficiency η_{coil} of 83.5% in good agreement with the EM simulations.

The coil system was connected on one side to the COTS power amplifier and on the other side to a 50 Ω load, which we found is the optimal load impedance for maximum power transfer efficiency. Fig. 12 illustrates the efficiency $\eta_{amp} \cdot \eta_{coil}$ and the power delivered to the 50 Ω load vs. misalignement angle. In the angular range ±15°, the power transfer efficiency $\eta_{amp} \cdot \eta_{coil}$ is higher than 76%, with a peak value of 80%.

To characterize the full-wave rectifier under high-power levels, the PA was directly connected to the input port of the rectifier. Its output port was connected to the buck converter with a load resistance of 6.5 Ω and no supercapacitors, measuring the efficiency $\eta_{amp} \cdot \eta_{rect} \cdot \eta_{buck}$ by varying the PA DC input voltage, as reported in Fig. 13. it can be seen that the desired output power of 3.9 W, corresponding to $12 \cdot P_{node}$, is achieved for DC input power of greater than 5 W. In this condition, by using the efficiencies η_{amp} and η_{buck} provided by the respective datasheets, equal to 91% and 96%, respectively, a rectifier efficiency η_{rect} of 80% is obtained. The efficiency η_{rect} is calculated using the module datasheet peak efficiencies for a conservative estimate of the rectifier performance.

Finally, the overall WPT link DC-DC efficiency was estimated connecting the buck converter output to the 6.5 Ω resistance and measuring the DC power delivered to the load. As reported in Fig. 14, the system features a constant transmission efficiency η_{wpt} of 58% for a misalignment up to 30°and the minimum value of 54% for a misalignment up to 40°. Therefore, using (5) with an angle α=40°, the minimum required load power P_{load} to be delivered during T_{tx} is 2.9 W instead of 3.9 W. Using the minimum efficiency measured inside the misalignment of ±20°, which is 54%, and (5), it is

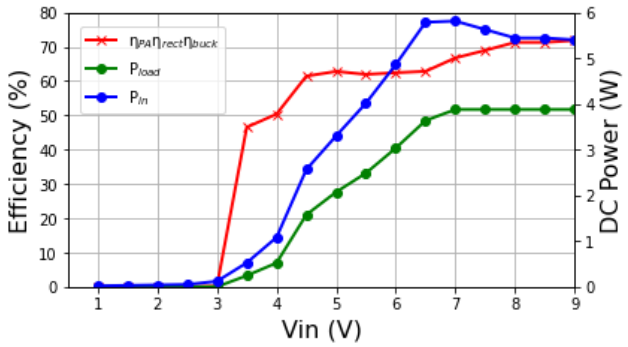

FIGURE 13. Measured AC/DC block efficiency and DC output power on the 6.5Ω load, and PA input power vs PA input voltage.

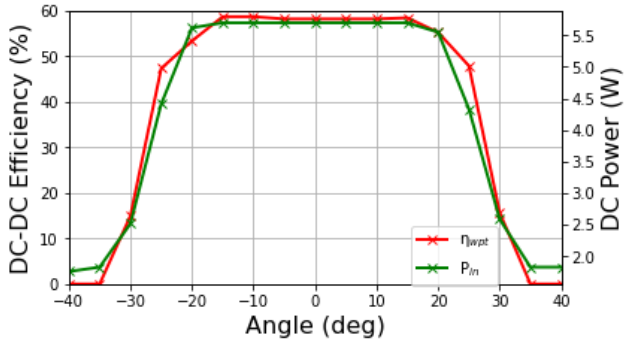

FIGURE 14. Measured dynamic DC-DC efficiency and input DC input power of the WPT system with a 6.5Ω load and PA HV voltage of 7.6 V.

required a minimum DC input power of 5.6 W to deliver about 3 W to the load.

IV. DYNAMIC MEASUREMENT

The proposed system was tested in a laboratory environment using the roll mock-up shown in Fig. 10, with the disk rotating at a frequency of about 4 Hz. The WPT receiver blocks were mounted on the disk, while, on the transmitter side, the PA was connected to the TX coil and supplied by a DC power supply. The TX coil, along with its holder, was placed on top of a support to ensure proper alignment with the RX coil at a distance $d = 2$ cm, as shown in Fig. 10 (b). To collect and process data, the static MCU was configured to receive the BLE packets and forward them to a computer using the Universal Asynchronous Receiver-Transmitter (UART) protocol. Data received over serial communication were saved and analysed using a Python script.

The PA HV voltage was set to 7.6 V as it was for the angular measurements reported in Fig. 14, resulting in an input power of 5.7 W for the coil overlapping condition. However, due to the coupling system border effects for misalignment greater than ±20°, the delivered energy to the load is higher than the required node energy E_{rev} thus overcharging the capacitors. If the load voltage reaches the threshold value of 5 V, the buck converter stops charging the capacitors, supplying only the node with a resistance R_{node}. Although this does not interfere with the node operation, it might cause harm to the WPT system. In fact, the sudden change of load resistance, from 6 Ω to 70 Ω, causes potential power reflection. Instead of increasing the buck converter threshold voltage, which would cause an increase in the node power consumption, the static MCU was programmed to switch on and off the PA drivers so that the voltage across the supercapacitors is in the range $[V_{lh}\text{-}V_{th}] = [4.3\text{-}4.5]$ V. To do so, a digital comparator with hysteresis was implemented inside the static MCU, using the measured voltage data transmitted by the node to control the PA via the active low enabling pin of the driver module.

Fig. 15 shows the measured data during a ten minutes test. During that period, voltage and angular data were continuously acquired and transmitted by the node regardless of the PA status. The load voltage value during the test is depicted in Fig. 15 (a). After an initial starting phase, the load voltage alternates charging and discharging periods to keep the voltage inside the defined operative range, proving the effectiveness of the digital comparator. The charging T_{ct} and discharging T_{dt} intervals last for about 33 s and 7 s, respectively. The angular position of the node, and thus the disk rotational speed, is shown in Fig. 15 (b). During an interval of 1 s, the disk made three complete revolutions and only 210° of the fourth, thus resulting in a rotational frequency of 3.6 Hz.

In terms of system efficiency, (4) should be modified to account for the energy stored inside the supercapacitors and thus define the WPT system energy efficiency. By considering the capacitors charging time *Tct* and stored energy to pass from 4.3 V to 4.5 V, we can define the capacitor energy variation ΔE_{cap}, the node energy consumption E_{ct}, and the energy provided at the PA input E_{in} as follow:

$$\Delta E_{cap} = \frac{1}{2} C (V_{th}^2 - V_{lh}^2) \tag{12}$$

$$E_{ct} = P_{node} T_{ct} \tag{13}$$

$$E_{in} = \frac{P_{in} T_{ct}}{\chi}. \tag{14}$$

Therefore, the WPT energy efficiency can be expressed as:

$$\eta_{E,wpt} = \frac{E_{ct} + \Delta E_{cap}}{E_{in}} \tag{15}$$

using $T_{ct} = 33$ s and the transmission angle of ± 20° the obtained system DC-DC energy efficiency is $\eta_{E,wpt}$=62%.

The system was tested at various rotating speeds to verify its correct operation at different machinery rotational frequencies, as shown in (5). If the rotational speed is higher, the transmitted energy and node required energy per round are lower, but the number of rotations in a given period is higher. The opposite occurs if the rotational speed is lower. Therefore, in a given period the transmitted energy is the same. This results in maintaining a consistent energy balance over time as shown Fig. 16 for measured data of 2 Hz (top) and 4 Hz (bottom) rotating speeds, respectively.

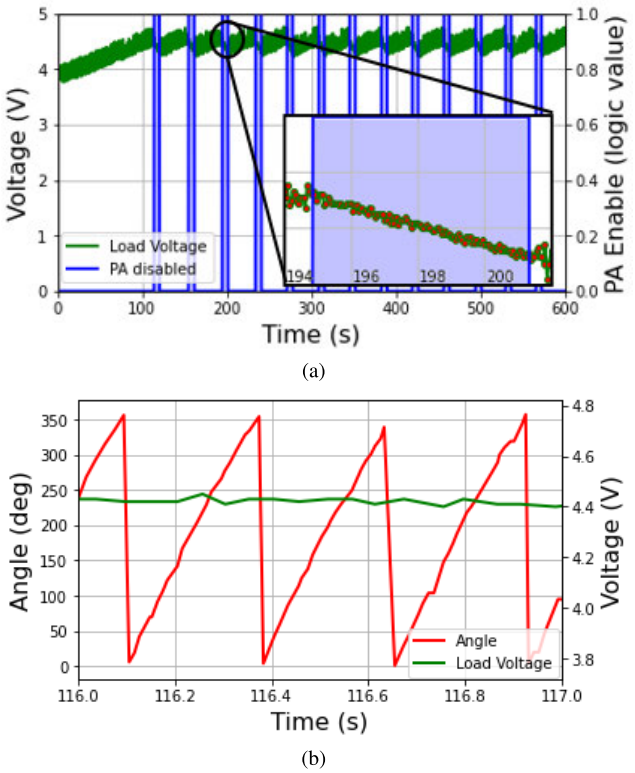

FIGURE 15. Experimental data measurement. (a) Load voltage and PA enable signal over the entire test, and (b) 1-second shoot of the measured load voltage and angular position. It can be seen that the disk is spinning at a frequency of 3.5 Hz.

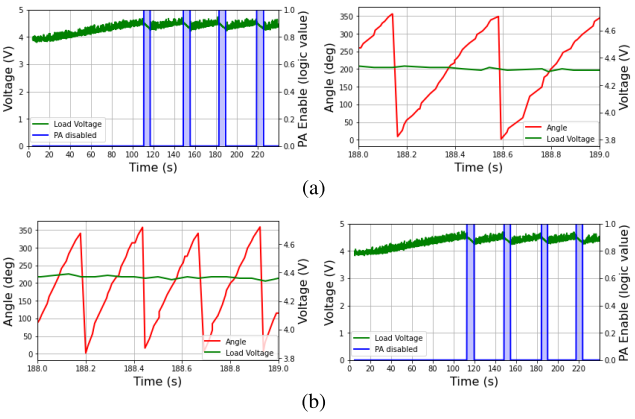

FIGURE 16. Experimental data measurement for different rotating speeds. (a) Load voltage, PA enable signal (left), and angular position (right) for a rotating speed of 2 Hz. (a) Load voltage, PA enable signal (left), and angular position (right) for a rotating speed of 4 Hz.

Concerning the minimum rotating frequency, the lower bound is set by the supercapacitors discharging time to pass from 4.5 V to 4.0 V during the period $T_{rev} - T_{tx}$. Indeed, if the voltage drops below that threshold when the coils are not aligned the node turns off, compromising the monitoring operations. In the adopted system, with the given supercapacitors and I_{node}, the minimum rotating frequency is about 50 mHz.

V. CONCLUSION

This paper presented a fully operational WPT system for a specific industrial condition monitoring representative of a class of applications, consisting of high-dimension industrial rotating equipment, that is of high interest in the area of Industrial IoT. By employing a pair of different planar coils that occupy only a section of the outer circular crown of the roll, a PWPT system has been designed and tested using rotating emulating equipment.

The reported comprehensive study of the magnetic coupling system has shown the benefit of using different coils for dynamic applications. Indeed, at the cost of a reasonable reduction in the coupling coefficient, the employment of different coils provides a wider and more stable link for WPT. In the specific case, using a series-series resonant topology, a power transfer efficiency η_{coil}>80% is maintained for a misalignment greater than ±20°. The developed PWPT system features a DC-DC efficiency η_{wpt} of 62% and can successfully power supply an IoT node provided with sensing and data transfer capability.

Thanks to its compact design, practical feasibility, and demonstrated effectiveness, this system introduces a novel approach to the design of a misalignment-tolerant magnetic coupling system, thereby paving the way for innovative dynamic WPT solutions.

REFERENCES

[1] Z. Zhang, H. Pang, A. Georgiadis, and C. Cecati, "Wireless power transfer—An overview," *IEEE Trans. Ind. Electron.*, vol. 66, no. 2, pp. 1044–1058, Feb. 2019.

[2] C. Liu, C. Jiang, J. Song, and K. T. Chau, "An effective sandwiched wireless power transfer system for charging implantable cardiac pacemaker," *IEEE Trans. Ind. Electron.*, vol. 66, no. 5, pp. 4108–4117, May 2019.

[3] Q. Ke, W. Luo, G. Yan, and K. Yang, "Analytical model and optimized design of power transmitting coil for inductively coupled endoscope robot," *IEEE Trans. Biomed. Eng.*, vol. 63, no. 4, pp. 694–706, Apr. 2016.

[4] C. C. Mi, G. Buja, S. Y. Choi, and C. T. Rim, "Modern advances in wireless power transfer systems for roadway powered electric vehicles," *IEEE Trans. Ind. Electron.*, vol. 63, no. 10, pp. 6533–6545, Oct. 2016.

[5] C.-C. Huang, C.-L. Lin, and Y.-K. Wu, "Simultaneous wireless power/data transfer for electric vehicle charging," *IEEE Trans. Ind. Electron.*, vol. 64, no. 1, pp. 682–690, Jan. 2017.

[6] A. P. Sample, D. T. Meyer, and J. R. Smith, "Analysis, experimental results, and range adaptation of magnetically coupled resonators for wireless power transfer," *IEEE Trans. Ind. Electron.*, vol. 58, no. 2, pp. 544–554, Feb. 2011.

[7] Y. Zhang, S. Chen, X. Li, and Y. Tang, "Design methodology of free-positioning nonoverlapping wireless charging for consumer electronics based on antiparallel windings," *IEEE Trans. Ind. Electron.*, vol. 69, no. 1, pp. 825–834, Jan. 2022.

[8] M. Wagih, A. Komolafe, I. Ullah, A. S. Weddell, and S. Beeby, "A wearable all-printed textile-based 6.78-MHz 15 W-output wireless power transfer system and its screen-printed Joule heater application," *IEEE Trans. Ind. Electron.*, pp. 1–10, 2023.

[9] W. Ejaz, M. Naeem, M. Basharat, A. Anpalagan, and S. Kandeepan, "Efficient wireless power transfer in software-defined wireless sensor networks," *IEEE Sensors J.*, vol. 16, no. 20, pp. 7409–7420, Oct. 2016.

[10] L. Li, H. Liu, H. Zhang, and W. Xue, "Efficient wireless power transfer system integrating with metasurface for biological applications," *IEEE Trans. Ind. Electron.*, vol. 65, no. 4, pp. 3230–3239, Apr. 2018.

[11] S. Jeong, D.-H. Kim, J. Song, H. Kim, S. Lee, C. Song, J. Lee, J. Song, and J. Kim, "Smartwatch strap wireless power transfer system with flexible PCB coil and shielding material," *IEEE Trans. Ind. Electron.*, vol. 66, no. 5, pp. 4054–4064, May 2019.

[12] V. F. Tseng, S. S. Bedair, and N. Lazarus, "Acoustic power transfer and communication with a wireless sensor embedded within metal," *IEEE Sensors J.*, vol. 18, no. 13, pp. 5550–5558, Jul. 2018.
[13] X. Liu, C. Liu, W. Han, and P. W. T. Pong, "Design and implementation of a multi-purpose TMR sensor matrix for wireless electric vehicle charging," *IEEE Sensors J.*, vol. 19, no. 5, pp. 1683–1692, Mar. 2019.
[14] L. Song, H. Wang, and P. Chen, "Vibration-based intelligent fault diagnosis for roller bearings in low-speed rotating machinery," *IEEE Trans. Instrum. Meas.*, vol. 67, no. 8, pp. 1887–1899, Aug. 2018.
[15] Y. Chi, Y. Dong, Z. J. Wang, F. R. Yu, and V. C. M. Leung, "Knowledge-based fault diagnosis in Industrial Internet of Things: A survey," *IEEE Internet Things J.*, vol. 9, no. 15, pp. 12886–12900, Aug. 2022.
[16] I. Bisio, C. Garibotto, A. Grattarola, F. Lavagetto, and A. Sciarrone, "Exploiting context-aware capabilities over the Internet of Things for Industry 4.0 applications," *IEEE Netw.*, vol. 32, no. 3, pp. 101–107, May 2018.
[17] H. Wu, H. Tian, G. Nie, and P. Zhao, "Wireless powered mobile edge computing for industrial Internet of Things systems," *IEEE Access*, vol. 8, pp. 101539–101549, 2020.
[18] A. Costanzo, D. Masotti, G. Paolini, and D. Schreurs, "Evolution of SWIPT for the IoT world: Near- and far-field solutions for simultaneous wireless information and power transfer," *IEEE Microw. Mag.*, vol. 22, no. 12, pp. 48–59, Dec. 2021.
[19] T. Fujita, T. Yasuda, and H. Akagi, "A dynamic wireless power transfer system applicable to a stationary system," *IEEE Trans. Ind. Appl.*, vol. 53, no. 4, pp. 3748–3757, Jul. 2017.
[20] C. Xu, Y. Zhuang, C. Song, Y. Huang, and J. Zhou, "Dynamic wireless power transfer system with an extensible charging area suitable for moving objects," *IEEE Trans. Microw. Theory Techn.*, vol. 69, no. 3, pp. 1896–1905, Mar. 2021.
[21] A. Azad, R. Tavakoli, U. Pratik, B. Varghese, C. Coopmans, and Z. Pantic, "A smart autonomous WPT system for electric wheelchair applications with free-positioning charging feature," *IEEE J. Emerg. Sel. Topics Power Electron.*, vol. 8, no. 4, pp. 3516–3532, Dec. 2020.
[22] Y. Liu, R. Mai, D. Liu, Y. Li, and Z. He, "Efficiency optimization for wireless dynamic charging system with overlapped DD coil arrays," *IEEE Trans. Power Electron.*, vol. 33, no. 4, pp. 2832–2846, Apr. 2018.
[23] A. Pacini, A. Costanzo, S. Aldhaher, and P. D. Mitcheson, "Design of a position-independent end-to-end inductive WPT link for industrial dynamic systems," in *IEEE MTT-S Int. Microw. Symp. Dig.*, Jun. 2017, pp. 1053–1056.
[24] Z. Yan, M. Wu, C. Zhao, Q. Hu, L. Zhu, L. Qiao, and L. Wang, "Free-rotation wireless power transfer system based on composite anti-misalignment method for AUVs," *IEEE Trans. Power Electron.*, vol. 38, no. 4, pp. 4262–4266, Apr. 2023.
[25] Z. Zhang and B. Zhang, "Angular-misalignment insensitive omnidirectional wireless power transfer," *IEEE Trans. Ind. Electron.*, vol. 67, no. 4, pp. 2755–2764, Apr. 2020.
[26] K. Shi, C. Tang, H. Long, X. Lv, Z. Wang, and X. Li, "Power fluctuation suppression method for EV dynamic wireless charging system based on integrated magnetic coupler," *IEEE Trans. Power Electron.*, vol. 37, no. 1, pp. 1118–1131, Jan. 2022.
[27] D.-W. Seo, "Comparative analysis of two- and three-coil WPT systems based on transmission efficiency," *IEEE Access*, vol. 7, pp. 151962–151970, 2019.
[28] L. Xiang, X. Li, J. Tian, and Y. Tian, "A crossed DD geometry and its double-coil excitation method for electric vehicle dynamic wireless charging systems," *IEEE Access*, vol. 6, pp. 45120–45128, 2018.
[29] International Telecommunication Union. (Sep. 2018). *R-REC-SM.1896-1-201809-I!!PDF-E*. [Online]. Available: https://www.itu.int/dms_pubrec/itu-r/rec/sm/R-REC-SM.1896-1-201809-I!!PDF-E.pdf
[30] A. J. Hanson, J. A. Belk, S. Lim, C. R. Sullivan, and D. J. Perreault, "Measurements and performance factor comparisons of magnetic materials at high frequency," *IEEE Trans. Power Electron.*, vol. 31, no. 11, pp. 7909–7925, Nov. 2016.
[31] H.-C. Chang, Y.-L. Hsu, S.-C. Yang, J.-C. Lin, and Z.-H. Wu, "A wearable inertial measurement system with complementary filter for gait analysis of patients with stroke or Parkinson's disease," *IEEE Access*, vol. 4, pp. 8442–8453, 2016.
[32] Dassault Systèmes. (2022). *CST Studio Suite*. [Online]. Available: https://www.3ds.com/products-services/simulia/products/cst-studio-suite/latest-release/
[33] S. Raju, R. Wu, M. Chan, and C. P. Yue, "Modeling of mutual coupling between planar inductors in wireless power applications," *IEEE Trans. Power Electron.*, vol. 29, no. 1, pp. 481–490, Jan. 2014.
[34] W. Li, H. Zhao, J. Deng, S. Li, and C. C. Mi, "Comparison study on SS and double-sided LCC compensation topologies for EV/PHEV wireless chargers," *IEEE Trans. Veh. Technol.*, vol. 65, no. 6, pp. 4429–4439, Jun. 2016.
[35] Keysight Technologies. (2022). *Advanced Design System (ADS)*. [Online]. Available: https://www.keysight.com/us/en/products/software/pathwave-design-software/pathwave-advanced-design-system.html

RAFFAELE SALVATI (Member, IEEE) was born in Foligno, Italy, in 1995. He received the B.Sc. and M.Sc. degrees in electronic engineering from the University of Perugia, in 2017 and 2020, respectively, where he is currently pursuing the Ph.D. degree in industrial and computer engineering. In 2023, he visited the Institut für Mechatronik, Innsbruck, Austria, and worked on RFID technologies for condition monitoring. His current research interests include wireless power transfer and wearable electronics along with sensing and energy harvesting.

VALENTINA PALAZZI (Senior Member, IEEE) received the M.S. degree in electrical engineering and the Ph.D. degree in industrial and information engineering from the University of Perugia, Italy, in 2014 and 2018, respectively.

In 2015, she was a Visiting Ph.D. Student with the Tyndall National Institute, Cork, Ireland; in 2016, she did a short-term scientific mission with the Centre Tecnològic de Telecomunicacions de Catalunya, Barcelona, Spain, sponsored by the cost action IC1301 "WiPE"; from December 2016 to April 2017, she was a student intern with the Agile Technologies for High- Performance Electromagnetic Novel Applications Research Group, School of Electrical and Computer Engineering, Georgia Institute of Technology, Atlanta, GA, USA. Since 2019, she has been a Researcher with the High Frequency Electronics Laboratory, Department of Engineering, University of Perugia, Italy. She has co-authored more than 50 articles, and holds three patents. Her current research interests include wireless sensors, radar front ends, wireless power transfer technologies, beamfomring networks, additive manufacturing processes, and conformal electronics.

Dr. Palazzi is an elected member of the IEEE Microwave Theory and Technique Society (MTT-S) Administrative Committee. She is the past chair (term 2022-2023) of the IEEE MTT-S Technical Committee- 26 "RFID, Wireless Sensor and IoT", and Early Career Representative of the URSI Commission D "Electronics and Photonics" of the International Union of Radio Science (URSI). She was a recipient of the First Place Award of the Student Design Competition on Wireless Energy Harvesting held at the 2016 IEEE MTT-S "International Microwave Symposium" (IMS), of the IEEE MTT-S Graduate Fellowship in 2017, of the 2017 MTT-S Prize - Italy Chapter Central and Southern Italy, of the URSI Young Scientist Best Paper Award confered at the 2019 URSI Italian National Meeting, of the Second Place at the 3 Minute Thesis Competition held at IMS 2021, and of the GAAS Young Scientist Recognition (URSI Commission D) confered at GASS 2021.

FEDERICO ALIMENTI (Senior Member, IEEE) received the Laurea degree (magna cum laude) and the Ph.D. degree in electronic engineering from the University of Perugia, Italy, in 1993 and 1997, respectively. Since 2001, he has been with the Department of Engineering, University of Perugia, teaching the class of RFIC design. From 2011 to 2014, he was the Scientific Coordinator of the ENIAC ARTEMOS Project. In Summer 2014, he was a Visiting Professor with EPFL, Switzerland. He has participated in the Summer School 2017, held at Infineon Austria AG, Villach, as a Keynote Lecturer. He is currently an Associate Professor of electronics. He has authored three European patents and more than 200 papers in journals/conferences and books. His H-index of 26 with more than 2000 citations (source Scopus). His research interests include microwave and RFIC design. In 1996, he was a recipient of the URSI Young Scientist Award and the Visiting Scientist from the Technical University of Munich, Germany. In 2013, he was also a recipient of the IET Premium (Best Paper) Award and the TPC Chair of the IEEE Wireless Power Transfer Conference. In 2018, he got the qualification as a ''Full Professor'' and won the ''Mario Sannino'' Award for the best research in the field of microwave electronics.

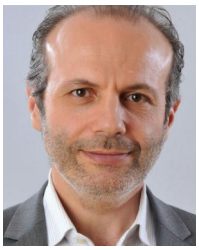

PAOLO MEZZANOTTE (Member, IEEE) was born in Perugia, Italy, in 1965. He received the Ph.D. degree from the University of Perugia, Perugia, in 1997. Since 2007, he has been an Associate Professor with the University of Perugia, where he has been involved in teaching the classes ''Radiofrequencies Engineering'' and ''Systems and Circuits for IoT.'' He was the Vice Head of the Department of Engineering, University of Perugia, from 2014 to 2019. These research activities are testified by more than 170 publications in the most reputed specialized journals and at the main conferences of the microwave scientific community. His present H-index is 22 (source Scopus). His current research interests include the development of microwave circuits on bio-compatible substrates and the enabling technologies for the IoT. He served as the Chair for the IEEE Technical Committee MTT-24-RFID Technologies for the biennium, from 2018 to 2019. He is currently the Chair of the IEEE Topical Conference on Wireless Sensors and Sensor Networks and an Associate Editor of *The Applied Computational Electromagnetics Society Journal* and IEEE JOURNAL OF MICROWAVES.

ANTONIO FABA (Senior Member, IEEE) received the Electrical Engineering degree from the University of L'Aquila, Italy, in 1998, and the Ph.D. degree in industrial engineering from the University of Perugia, Italy, in 2006. He is currently an Associate Professor with the Department of Engineering, University of Perugia, Italy, where he is the Head of the Laboratory of Electromagnetic Characterization. He is a member of the IEEE Magnetic Society. He received the National Habilitation for a Full Professor, in 2018.

ERMANNO CARDELLI (Senior Member, IEEE) received the Ph.D. degree in electrical engineering from the University of Pisa. Currently, he is a Full Professor of electric engineering with the University of Perugia and the Head of the Department of Engineering. He is a Professional Engineer. He is the author of more than 200 refereed technical articles, mainly on numerical techniques and modeling for electromagnetic field analysis. Authors of two Italian-edited books and an international book chapter. He was the past Chair of the IEEE Italy Section. He was the general chair of several international conferences and a coordinator of many Italian and European Scientific Programs. The Chair of the Electrical Engineering (ET) Group. He was a referee and the guest editor of international journals.

LUCA ROSELLI (Fellow, IEEE) joined the University of Perugia, Perugia, Italy, in 1991. In 2000, he founded the spin-off WiS Srl, Foligno, Italy. He was a member of the Board of Directors of ART Srl, Urbino, Italy, from 2008 to 2012. He was involved in electronic technologies for the Internet of Things for six years. He is currently a Qualified Full Professor with the University of Perugia, where he teaches applied electronics and coordinates the High Frequency Electronics Laboratory. He has authored more than 280 articles (H-index 23, i10 51, and more than 2200 citations: Scholar) and *Green RFID System* (Cambridge University Press, 2014). His current research interests include HF electronic systems with special attention to RFID, new materials, and wireless power transfer.

He is a member of the list of experts of Italian Ministry of Research, the past Chair of the IEEE Technical Committees MTT-24-RFID, the Vice-Chair of the 25-RF Nanotechnologies, the 26-Wireless Power Transfer, the ERC Panel PE7, and the Advisory Committee of the IEEE-WPTC, and the Chairperson of the SC-32 of IMS. He is also the Co-Chair of the IEEE Wireless Sensor Network Conference. He organized the VII Computational Electromagnetic Time Domain, in 2007, and the First IEEE Wireless Power Transfer Conference, in 2013. He is an Associate Editor of *IEEE Microwave Magazine*. He is involved on the boards of several international conferences. He is a Reviewer of many international reviews, including PROCEEDINGS OF THE IEEE, IEEE TRANSACTIONS ON MICROWAVE THEORY AND TECHNIQUES, and IEEE MICROWAVE AND WIRELESS COMPONENTS LETTERS.

Open Access funding provided by 'Università degli Studi di Perugia' within the CRUI CARE Agreement